JBM J Bone Metab 2014;21:117-126
http://dx.doi.org/10.11005/jbm.2014.21.2.117
pISSN 2287-6375 eISSN 2287-7029

Review Article

Can Dental Cone Beam Computed Tomography Assess Bone Mineral Density?

Do-Gyoon Kim

Division of Orthodontics, Ohio State University College of Dentistry, Columbus, OH, USA

Corresponding author
Do-Gyoon Kim
Division of Orthodontics, College of Dentistry
The Ohio State University 4088 Postle Hall
305 W. 12th Ave Columbus, OH 43210 USA
Tel: +614-247-8089
Fax: +614-688-3077
E-mail: kim.2508@osu.edu

Received: April 3, 2014
Revised: May 18, 2014
Accepted: May 18, 2014

No potential conflict of interest relevant to this article was reported.

The author thanks his student, Trenton B. Johnson, for helpful discussions about the subjects described in this review.

Mineral density distribution of bone tissue is altered by active bone modeling and remodeling due to bone complications including bone disease and implantation surgery. Clinical cone beam computed tomography (CBCT) has been examined whether it can assess oral bone mineral density (BMD) in patient. It has been indicated that CBCT has disadvantages of higher noise and lower contrast than conventional medical computed tomography (CT) systems. On the other hand, it has advantages of a relatively lower cost and radiation dose but higher spatial resolution. However, the reliability of CBCT based mineral density measurement has not yet been fully validated. Thus, the objectives of this review are to discuss 1) why assessment of BMD distribution is important and 2) whether the clinical CBCT can be used as a potential tool to measure the BMD. Brief descriptions of image artefacts associated with assessment of gray value, which has been used to account for mineral density, in CBCT images are provided. Techniques to correct local and conversion errors in obtaining the gray values in CBCT images are also introduced. This review can be used as a quick reference for users who may encounter these errors during analysis of CBCT images.

Key Words: Artifacts, Bone density, Calibration, Cone-beam computed tomography, Radiation

Why assessment of bone mineral density (BMD) distribution is important?

Bone is a connective tissue designed to bear loading generated by muscle movement and body weight during daily activity.[1,2] Bone in a live skeletal system constantly changes. Approximately 7.5% of bone turnover occurs annually.[3] Bone modeling and remodeling are inherently involved in the alteration of bone. In the process of bone remodeling, a bone resorbing cell, osteoclast, is activated to remove the pre-existing bone tissue and subsequently, new bone is deposited by a bone forming cell, osteoblast.[3-7] The bone modeling is an uncoupled process consisting of activation and resorption or activation and formation. When bone resorption and formation are balanced, the net quantity of bone is maintained. It has been observed that bone quantity is associated with its mechanical strength.[8,9] As bone in a live patient cannot be subject to mechanical testing, many non-invasive imaging technologies have been developed to estimate the bone quantity as a surrogate for a patient's bone fragility. Computed tomography (CT) has

been widely used non-invasive device to assess bone mass.[10,11] This X-ray based tool mainly detects mineral, which is the densest component in bone tissue materials, and provides Hounsfield units (HU) as the measures. It is well known that bone is composed of approximately 30% water, 40% mineral, and 30% organic protein (mostly collagen) at the tissue level.[1] In the initial process of bone formation, osteoblasts produce immature collagen and mineral composite.[12] The mineral content rapidly increases up to 70% of full mineralization within one week post-initiation of bone formation.[13] Following the first mineralization, more minerals are added to the collagen-mineral composite during the secondary mineralization process that lasts for years.[13,14] Bone modeling and remodeling processes are activated at different time points. In particular, active bone remodeling is stimulated by bone disease and complications including estrogen deficiency in postmenopausal osteoporosis, osteoarthritis, fracture healing, and implantation surgery.[2,6,7,15-18] As a result, heterogeneity of bone tissue mineral density (TMD) increases (Fig. 1).

BMD accounts for bone quantity as the mineral contents within an apparent volume of bone, which includes porosity, bone marrow, as well as bone matrix. On the other hand, the TMD represents mineral contents only in the matrix of bone.[18,19] Bone quantity measurements have been widely used to diagnose bone disease. For example, according to the World Health Organization (WHO) criteria, osteoporosis is defined as 2.5 standard deviations or more below the average value for young healthy women.[20,21] However, it has been indicated that bone quantity alone cannot explain bone fragility.[20,22] On the other hand, the bone quality is assessed by its morphology and TMD distribution.[23,24] Mechanical properties of trabecular bone are explained using three-dimensional (3D) morphological parameters of trabecular bone such as trabecular number, thickness, and anisotropy ratio.[25-27] Recently, many studies have also indicated that TMD is responsible for controlling elastic, plastic, and viscoelastic mechanical properties at the tissue level of bone.[28-31] As such, efforts have been made to develop a new imaging technology that can non-invasively assess the bone quality. Dual energy X-ray absorptiometry (DXA) has been recognized as a standard technique to obtain the BMD of a patient's spine or hip clinically. However, the DXA produces a low resolution (approximately 500 μm [32]) 2D image that only provides areal BMD and cannot precisely delineate cancellous bone structure with the trabecular thickness level of 50 to 200 μm.[25,33,34] A high-resolution (up to less than 1 μm) 3D micro-CT image can describe detailed bone morphology and TMD more accurately than other CT images (Fig. 2). However, much higher radiation doses are generated during the longer scanning time of micro-CT for the same size of a specimen, which limits its use to laboratory

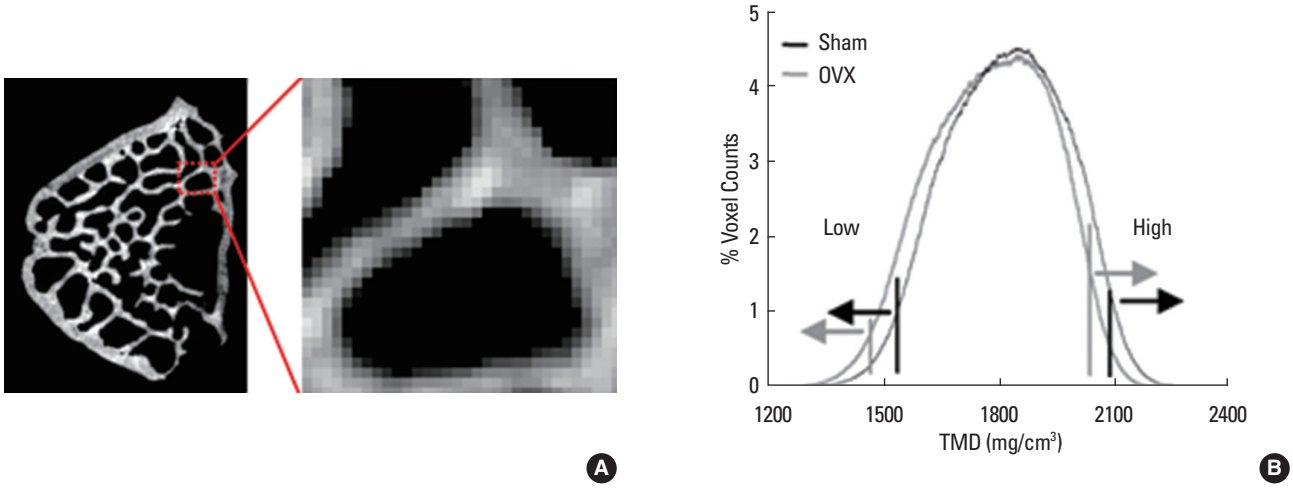

Fig. 1. (A) Detailed tissue mineral density (TMD) distribution in vertebral trabecular bone. A darker color represents less TMD. (B) A typical TMD histogram of a micro-computed tomography image (voxel size 16×16×16 μm^3). The TMD distribution was different between the control sham surgery (black) and ovariectomized (OVX) (gray) groups. [Reprinted from "Increased variability of bone tissue mineral density resulting from estrogen deficiency influences creep behavior in a rat vertebral body", by Kim DG, Navalgund AR, Tee BC, Noble GJ, Hart RT, Lee HR, 2012, Bone, 51(5), pp. 868-75. Copyright 2012 by the Elsevier. Reprinted with permission].

http://dx.doi.org/10.11005/jbm.2014.21.2.117

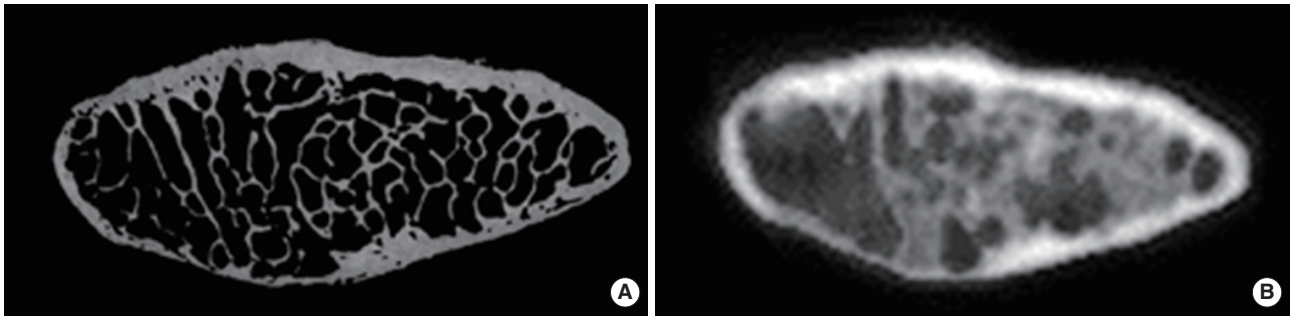

Fig. 2. (A) Micro-computed tomography (CT) image (27×27×27 μm^3 voxel size) and (B) cone beam CT image (200×200×200 μm^3 voxel size) of the same human condyle.

Table 1. Descriptive summary of X-ray based technologies [10, 32, 41, 80-82]

Technologies	Voxel size (μm)	Effective radiation dose (μSv)	Scan time (second)	References
DXA	500	1–20	-120	[10, 32, 82]
MDCT	156–500	100–8,000	<30	[80, 82]
CBCT	130–400	6.3–2,100	10–40 (Rotation) 1.92–7.2 (Exposure)	[41, 81]
Micro-CT	0.3–100	NA	>600	[80]

DXA, dual-energy X-ray absorptiometry; MDCT, multidetector computed tomography; CBCT, cone beam computed tomography; Micro-CT, micro-computed tomography.

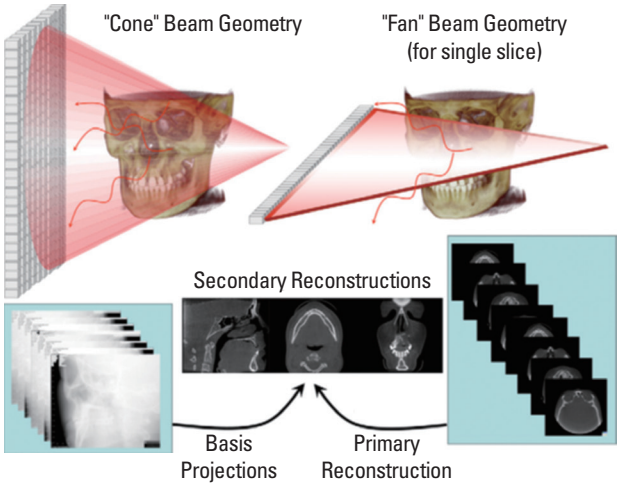

Fig. 3. X-ray beam projection scheme comparing acquisition geometry of conventional or "fan" beam (right) and "cone" beam (left) imaging geometry and resultant image production. The amount of scatter generated (sinusoidal lines) and recorded by cone-beam image acquisition is substantially higher, reducing image contrast and increasing image noise. [Reprinted from "What is cone-beam CT and how does it work?", by Scarfe WC, Farman AG, 2008, Dent Clin North Am, 52(4), pp.707-30. Copyright 2008 by the Elsevier. Reprinted with permission].

research purposes only. On the other hand, cone beam CT (CBCT) provides higher image resolution with less radiation dose and exposure time than the conventional clinical multidetector CT (MDCT) (Table 1). Thus, CBCT has been widely used for the clinical diagnosis of dental complications.[35,36] The 3D image produced by CBCT allows for detailed morphological analysis of bone. However, reliability of CBCT based bone density measurement remains to be determined.[37-39] Thus, this review will discuss whether the CBCT can be used to assess BMD at next sections.

1. How a CBCT image is created?

The CBCT is relatively recent technology, with the first commercial scanner being introduced in 1998 for dental imaging.[40] This is a type of CT that uses a cone X-ray beam instead of the conventional fan beam (Fig. 3).[35] For standard full field of view for CBCT, polychromatic X-rays are generated from a source tube excited by 100-120 kV tube potential with 1.5-10 mA current.[41] The emitted X-ray photon energy is absorbed by materials located between the X-ray source and detector. The remaining energy after absorption is recorded on a detector as expressed by intensity (I) that represents energy per area and time. For example, the flat-panel detector consists of a pixel array of hydrogenated amorphous silicon thin-film transistors.[35] A scintillating material (e.g., Gd_2O_2S) detects the X-rays and converts them into visible light that is charged in the pixel transistors. A CT attenuation coefficient value of the material can be obtained by the Lambert-Beer law (Eq. 1).[39]

$$I = I_0 \exp[-\int \mu dL] \quad \text{(Eq. 1)}$$

where I_0 is the intensity emitted by the source, μ represents the attenuation coefficient, and l is a distance over which the attenuation is integrated. A denser material ab-

sorbs more energy resulting in a higher attenuation value. The attenuation values are converted to gray values in a digital (8-bit to 16-bit) image while the scanned image slices are reconstructed. As such, the gray value in the CBCT image is theoretically equivalent to the density of the material. However, in order to obtain a reliable density value using a CBCT image, multiple factors must be considered.

2. CBCT artefacts from machine factors

Imaging artefacts associated with general CT systems also occur in CBCT imaging.[39,42,43] Referring to the artefacts listed in previous literatures, this review summarizes the artefacts that can influence the CBCT based bone density measurements and related issues.

1) Noise

This artefact is appeared as inconsistent gray values with large standard deviations. This result arises from low signal-to-noise ratio of intensity, which needs to maintain the low radiation dose. The noise level can be reduced by increasing the excitation potential and current.

2) Scatter artefacts

Scattered X-ray photons from the original path can be added to the primary intensity giving rise to an underestimation of attenuation value in Eq. 1. Larger detectors have a greater chance of encountering the scattered X-ray photons leading to streak artefacts during reconstruction process for the CBCT image.

3) Beam hardening

As the energy levels of polychromatic X-ray beams used in the CBCT are not identical, the lower energy photons can be easily absorbed at the edges of the scanned subject resulting in hardening of the X-ray beam, which produces lower gray values toward the center of the subject (cupping artifact) even if the density of the subject is homogenous.

4) Ring artefacts

Defects or uncalibrated components in the detector may cause ring artefacts with concentric rings in the CBCT image. The ring voxels have inconsistent gray values that can increase overall errors in the assessment of bone density.

5) Partial volume effects

The cubic or rectangular voxels cannot completely delineate the irregular shapes of scanned subjects. Thus, the gray value of voxels at the border between different density materials contains averaged attenuations. If the voxel size of CBCT image increases, it has more incorrect partial volume gray values.

3. CBCT artefacts from software factors

1) Reconstruction algorithm

A sinogram is constructed using digital signals from the pixel transistors. This composite image combines each row of each projection in the CBCT image.[35] Then, a mathematical algorithm converts the sinogram to 2D image slices and reconstructs them to a 3D CBCT image. The most predominantly used algorithm is a convolution-backprojection formula introduced by Feldkamp et al. [35,44] It was indicated that this backprojection algorithm causes unavoidable distortion in the transverse direction and resolution degradation in the longitudinal direction.[35] The reconstruction process also converts the raw intensity values in the sinogram to the gray values in the scale range of image data. Thus, absolute gray values may be different depending on the data size of the CBCT image utilized by the operation software of a CBCT machine company.

2) Field of view (FOV)

CBCT can improve the image resolution by reducing the FOV while decreasing overall radiation dose. However, variability of gray values is increased by using a smaller FOV (5 cm) compared to larger FOVs (10 to 20 cm).[38] Many other studies have indicated the FOV associated effects on gray value variability.[45,46]

3) HU

The attenuation coefficients of the same material scanned by different CT systems can vary if the scanning conditions are not identical. As the HU can be computed relative to the attenuation coefficient of water (Eq. 2), it has been widely used to compare material density between different CT systems.

$$HU = (\mu_{material} - \mu_{water}) / \mu_{water} \times 1000 \quad \text{(Eq. 2)}$$

It was suggested that the HU should be calibrated in order to obtain a consistent density value when the same material is scanned using different CT systems.[47,48]

http://dx.doi.org/10.11005/jbm.2014.21.2.117

However, accuracy of the CBCT based HU measurement still remains controversial.[37-39]

4. CBCT artefacts from patient factors

1) Streak artefact

Scanning dense metallic materials can cause severe streaking artifacts when their gray values exceed the maximum level of operation that the software can handle.[43] This artefact limits analysis of local gray values surrounding dental restorations and metal implants in patients. Other sources to cause streak artefacts include beam hardening, noise, and photon starvation that can appear when insufficient photons reach the detector.

2) Patient Motion

Shading or streaking artefacts may be observed when the gray values are incorrectly registered due to patient motion during CBCT scanning.[39,43] This artefact commonly appears as double contours in the CBCT image.

Can the clinical CBCT be used as a potential tool to measure the BMD?

Noise, ring and streak artefacts can be corrected by improving reconstruction algorithms.[39,42,49] Recently, a scatter-correction algorithm was developed to significantly improve the consistency of CBCT gray values including compressed sensing reconstruction algorithms to create a scatter-free CBCT image.[50,51] As the beam hardening effect is the most frequently observed artefact in CT scanning, many efficient correction algorithms have been developed and included in commercial CT software.[52,53] The FOV associated variations may arise because the back-projection algorithm includes gray values of tissues outside the small FOV during reconstruction.[39] Taken together, the recently improved reconstruction process likely corrects the local errors of gray value in the CBCT image. However, as these advanced algorithms need to be verified and calibrated to individual CT systems prior to being utilized in the clinical settings, the artefacts may be still observed in most of the currently used CT machines.

While the local errors can be visually detected, there are some systematic complications to be considered for CBCT based mineral density measurement. The most debated aspect is that the HU values of subjects are not consistent between different CT systems and between different times scanned even using the same CT system. These discrepancies can arise from the non-uniform process of scaling the HU values during reconstruction. It was indicated that a manufacturer's software imports a gray value range of 1 to 4,096 and rescales from -1,024 to 3,072.[47] This image would have 12-bit data size (2^{12}= 4,096). The gray value of an image with 8-bit data size is scaled from 0 to 255 (2^{8}= 256). The HU of water and air should be close to 0 and -1,000, respectively. However, the different scaling processes may provide completely different absolute values of HU

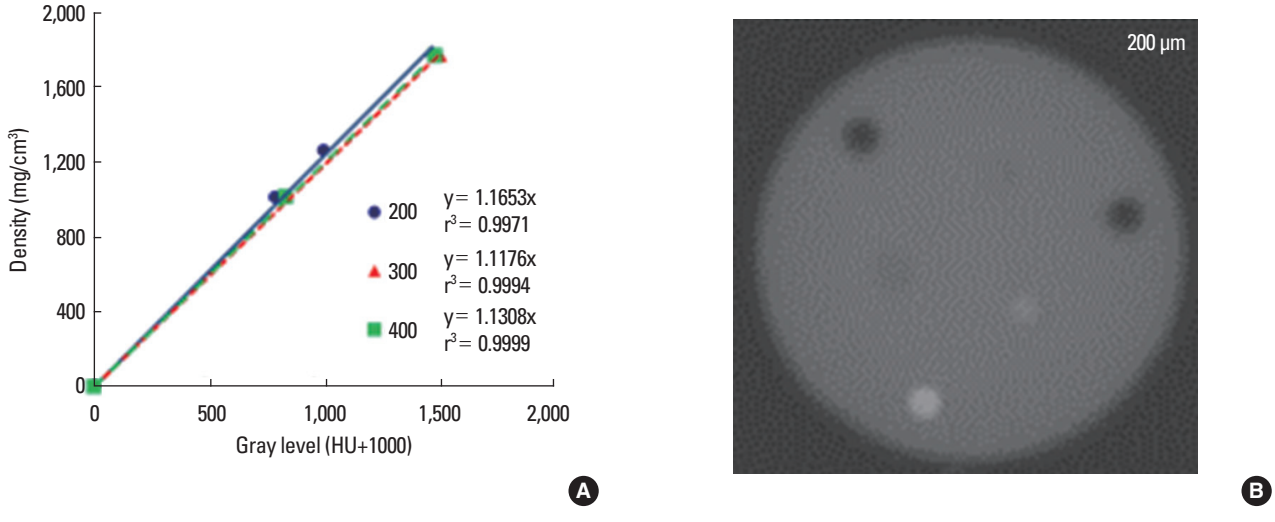

Fig. 4. (A) Strong positive correlations in the calibration curves of gray values for (B) phantoms of bone materials (hydroxyapatite) with 3 different densities (1,000, 1,250, and 1,750 mg/cm^3) scanned using 3 different resolutions (200, 300, and 400 μm) of cone beam computed tomography. HU, Hounsfield units.

for the same material. As such, the value of each voxel in a CBCT image may better represent the gray value rather than the HU.

Many studies found that strong positive correlations of the gray values of CBCT image with known density of reference materials and gray values obtained from the conventional clinical CT.[47,48,54-59] For example, phantoms of bone materials (hydroxyapatite) with 3 different densities (1,000, 1,250, and 1,750 mg/cm^3) were scanned using 3 different resolutions (200, 300, and 400 μm) of CBCT (Fig. 4). As a result, the CBCT based gray values of phantoms had strong positive correlations with the density values. The gray value of scanned specimens can be directly converted to the corresponding mineral density value using this calibration curve when the same CBCT scanner is used. Alternatively, a previous study found that the CBCT gray value strongly correlated with the CT attenuation coefficient (μ) of standard materials, which include aluminium (μ=0.678), outer bone equivalent (μ=0.523), inner bone equivalent (μ=0.255), polymethylmethacrylate (PMMA) (μ=0.220), muscle equivalent (μ=0.205), water equivalent (μ=0.202), adipose equivalent (μ=0.176), and air (μ=0.000).[47] Then, the corrected HU value of scanned materials was derived by estimating the attenuation values in the HU equation (Eq. 2) using the correlation equation with the CBCT gray values. The corrected HU values were comparable between different CBCT scanners. Recently, clinical applicability of this HU correction was validated using intraoral phantoms for patients.[48]

The aforementioned methods need external standard phantoms to be scanned to obtain the calibration curve. Another methodology was introduced using an internal reference to compare the mineral density between patients.[60,61] In the previous study using CBCT images of human cadaveric mandibles,[61] teeth were digitally separated from the mandible segment using imaging software

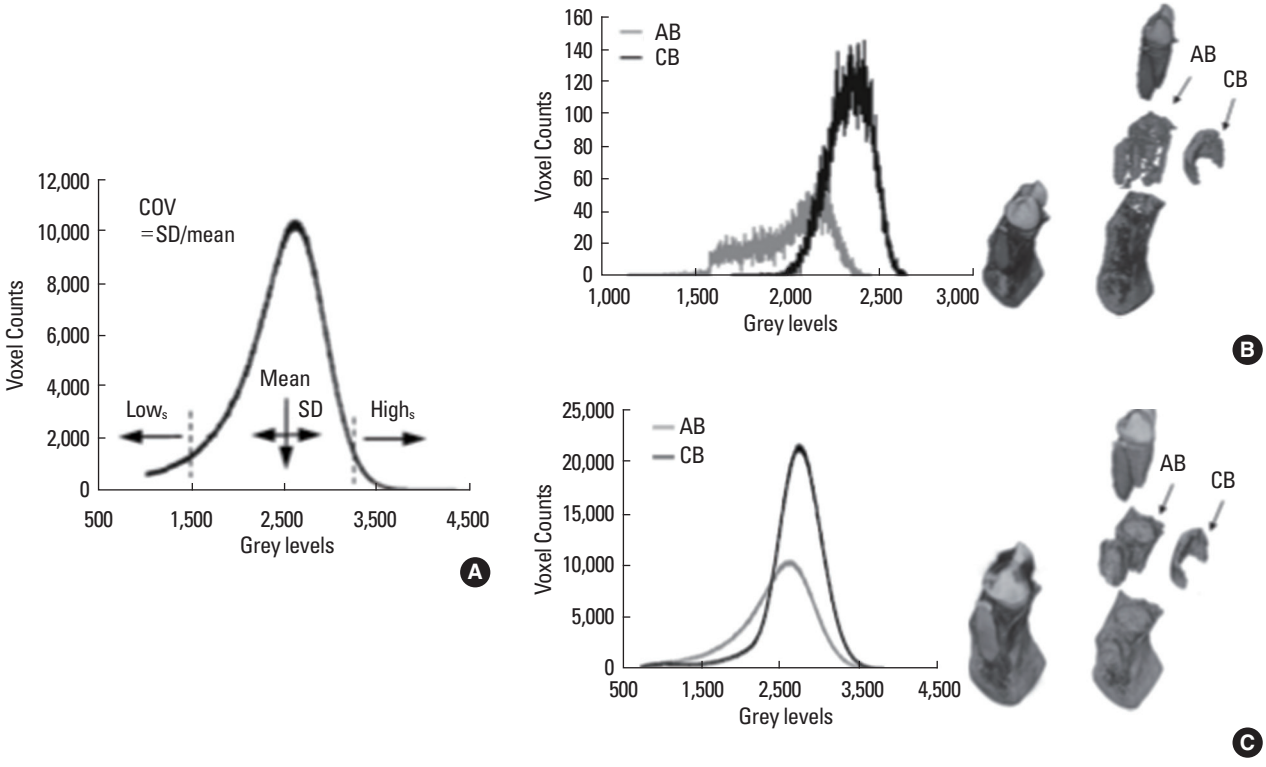

Fig. 5. (A) Degree of bone mineralization parameters determined using a grey level histogram, (B) comparison of grey level histograms between alveolar bone (AB, grey line) and basal cortical bone (CB, black line) regions using a three-dimensional (3D) cone beam computed tomography (CT) image (200×200×200 μm^3 voxel size), and (C) using 3D micro-CT image (20×20×20 μm^3 voxel size) for the same specimen. COV, coefficient of variation; High$_s$, grey level at the 95th percentile; LOW$_s$, grey level at the 5th percentile; SD, standard deviation; AB, alveolar bone; CB, control bone. [Modified from "Comparison of micro-CT and cone beam CT-based assessments for relative difference of grey level distribution in a human mandible" by Taylor TT, Gans SI, Jones EM, Firestone AR, Johnston WM, Kim DG, 2013, Dentomaxillofac Radiol, 42(3), pp. 25117764. Copyright 2013 by British Institute of Radiology. Reprinted with permission].

http://dx.doi.org/10.11005/jbm.2014.21.2.117

(Livewire®,[62] Institute of Computing, State University of Campinas, Brazil[61] and ImageJ, National Institutes of Health, Bethesda, Maryland, USA) (Fig. 5). The alveolar bone (AB) region was digitally isolated from within 1 mm of the root surface and the basal control bone (CB) was determined at 0.6 mm from periosteal and endosteal surfaces of the basal bone. The gray value histogram was used to obtain mean, standard deviation (SD), coefficient of variation (COV=SD/Mean), low and high gray values (Low5 and High5) at the 5th and the 95th percentiles of voxel counts in the histogram. The gray value parameters of the CB region were used as the internal references to compare those of AB region between subjects. It was assumed that a core region of basal cortical bone has normal bone remodeling while the AB and marginal basal bone regions have a rapid bone turnover due to active bone formation.[17,63] Percentage difference (%) of these gray level parameters between AB and basal cortical bone ([AB-CB]/[(AB+CB)/2]×100) was then computed for each patient CBCT image. The same image process was performed using the micro-CT images of the same human mandibles. As a result, the relative values of percentage differences were comparable between CBCT and micro-CT images based analyses. Those procedures to assess the gray value parameters were also applied to examine CBCT images collected from routine patients in clinic. An advantage of this method is that the relative value of the percentage difference is computed using the gray values of different regions in the same CBCT image avoiding the effects of different scanning conditions. The gray value histogram analyses were successfully used for clinical investigation of the success and failure of dental grafting and implant systems.[64,65]

To date, CBCT based BMD measurement has been used mainly to estimate bone properties for dental implantation.[66-70] The BMD measured from CBCT images showed a better predicting power to estimate cortical bone fracture than assessed by the conventional DXA images.[71] More applications are performed for the diagnosis of oral bone disease, improvement of orthodontic treatment, and maxillofacial surgery.[36,72-74] It is clear that higher resolution of 3D images can provide more useful information. For example, the partial volume effect can be reduced using a smaller voxel size in the image. However, if longer scanning time is required to obtain higher image resolution, the risk of high radiation exposure likely increases against the principle of "as low as reasonably achievable" (ALARA) radiation dose. As complete segmentation of bone voxels from non-bone voxels in the CT image with the current resolution can tremendously improve the capability of CT based analyses for both morphology and density (Fig. 2), numerous studies have been attempted to develop innovative algorithms.[75-78] Most commercialized CBCT software uses a global thresholding gray value to segment voxels. However, this simple method does not provide sufficient quality of images.[79] Further studies are still required to develop an optimal segmentation technology specific to individual CT images.

CONCLUSION

Mineral density distribution of bone tissue reflects the result of biological activity, which is altered due to bone complications. Clinical CT is an indirect method to measure mineral density distribution based on the X-ray attenuation coefficient of the materials, mainly the mineral, in bone tissue. Hence, CT based density measurement is not as accurate as direct measurement using biopsy. However, it is a very powerful non-destructive tool that allows for longitudinal diagnoses of patients' bone disease. Most of the local artefacts can be corrected by improving the CBCT image reconstruction algorithm and alternative corrective methods can be applied as visualized in the image. However, the image processing errors during converting the attenuation coefficient values to the HUs and gray values should be accurately addressed in order to compare the mineral density in CBCT images scanned under different conditions. This review briefly introduces the types of artefacts that occur and solutions to correct them as a quick reference for users who may find these errors in CBCT images.

REFERENCES

1. Martins RB, Burr DB, Sharkey NA. Skeletal tissue mechanics. New York, NY: Springer; 1998.
2. Carter DR, Beaupré GS. Skeletal function and form: mechanobiology of skeletal development, aging, and regeneration. New York, NY: Cambridge University Press; 2007.
3. Parfitt AM. The physiologic and clinical significance of

bone histomorphometric data. In: Recker R, editor. Bone histomorphometry: techniques and interpretations. Boca Raton, FL: CRC Press; 1983. p.143–223.
4. Allen MR, Turek JJ, Phipps RJ, et al. Greater magnitude of turnover suppression occurs earlier after treatment initiation with risedronate than alendronate. Bone 2011;49:128-32.
5. Kim DG, Shertok D, Ching Tee B, et al. Variability of tissue mineral density can determine physiological creep of human vertebral cancellous bone. J Biomech 2011;44:1660-5.
6. Turner RT, Riggs BL, Spelsberg TC. Skeletal effects of estrogen. Endocr Rev 1994;15:275-300.
7. Lerner UH. Bone remodeling in post-menopausal osteoporosis. J Dent Res 2006;85:584-95.
8. Keaveny TM, Hayes WC. A 20-year perspective on the mechanical properties of trabecular bone. J Biomech Eng 1993;115:534-42.
9. Keaveny TM. Biomechanical computed tomography-noninvasive bone strength analysis using clinical computed tomography scans. Ann N Y Acad Sci 2010;1192:57-65.
10. Genant HK, Engelke K, Fuerst T, et al. Noninvasive assessment of bone mineral and structure: state of the art. J Bone Miner Res 1996;11:707-30.
11. Genant HK, Jiang Y. Advanced imaging assessment of bone quality. Ann N Y Acad Sci 2006;1068:410-28.
12. Boonrungsiman S, Gentleman E, Carzaniga R, et al. The role of intracellular calcium phosphate in osteoblast-mediated bone apatite formation. Proc Natl Acad Sci U S A 2012;109:14170-5.
13. Roschger P, Paschalis EP, Fratzl P, et al. Bone mineralization density distribution in health and disease. Bone 2008;42:456-66.
14. Boivin G, Meunier PJ. Methodological considerations in measurement of bone mineral content. Osteoporos Int 2003;14 Suppl 5:S22-8.
15. Lee BC, Yeo IS, Kim DJ, et al. Bone formation around zirconia implants combined with rhBMP-2 gel in the canine mandible. Clin Oral Implants Res 2013;24:1332-8.
16. Kim DG, Huja SS, Tee BC, et al. Bone ingrowth and initial stability of titanium and porous tantalum dental implants: a pilot canine study. Implant Dent 2013;22:399-405.
17. Ames MS, Hong S, Lee HR, et al. Estrogen deficiency increases variability of tissue mineral density of alveolar bone surrounding teeth. Arch Oral Biol 2010;55:599-605.
18. Kim DG, Navalgund AR, Tee BC, et al. Increased variability of bone tissue mineral density resulting from estrogen deficiency influences creep behavior in a rat vertebral body. Bone 2012;51:868-75.
19. Renders GA, Mulder L, van Ruijven LJ, et al. Degree and distribution of mineralization in the human mandibular condyle. Calcif Tissue Int 2006;79:190-6.
20. McCreadie BR, Goldstein SA. Biomechanics of fracture: is bone mineral density sufficient to assess risk? J Bone Miner Res 2000;15:2305-8.
21. Genant HK, Cooper C, Poor G, et al. Interim report and recommendations of the World Health Organization Task-Force for Osteoporosis. Osteoporos Int 1999;10:259-64.
22. Heaney RP. Is the paradigm shifting? Bone 2003;33:457-65.
23. Hernandez CJ, Keaveny TM. A biomechanical perspective on bone quality. Bone 2006;39:1173-81.
24. Donnelly E. Methods for assessing bone quality: a review. Clin Orthop Relat Res 2011;469:2128-38.
25. Kim DG, Christopherson GT, Dong XN, et al. The effect of microcomputed tomography scanning and reconstruction voxel size on the accuracy of stereological measurements in human cancellous bone. Bone 2004;35:1375-82.
26. Hou FJ, Lang SM, Hoshaw SJ, et al. Human vertebral body apparent and hard tissue stiffness. J Biomech 1998;31:1009-15.
27. Morgan EF, Keaveny TM. Dependence of yield strain of human trabecular bone on anatomic site. J Biomech 2001;34:569-77.
28. Kim DG, Huja SS, Lee HR, et al. Relationships of viscosity with contact hardness and modulus of bone matrix measured by nanoindentation. J Biomech Eng 2010;132:024502.
29. Kim DG, Huja SS, Navalgund A, et al. Effect of estrogen deficiency on regional variation of a viscoelastic tissue property of bone. J Biomech 2013;46:110-5.
30. Isaksson H, Nagao S, Małkiewicz M, et al. Precision of nanoindentation protocols for measurement of viscoelasticity in cortical and trabecular bone. J Biomech 2010;43:2410-7.
31. Isaksson H, Malkiewicz M, Nowak R, et al. Rabbit cortical bone tissue increases its elastic stiffness but becomes less viscoelastic with age. Bone 2010;47:1030-8.
32. Guermazi A, Mohr A, Grigorian M, et al. Identification of vertebral fractures in osteoporosis. Semin Musculoskelet Radiol 2002;6:241-52.
33. Uchiyama T, Tanizawa T, Muramatsu H, et al. A morpho-

 http://dx.doi.org/10.11005/jbm.2014.21.2.117

metric comparison of trabecular structure of human ilium between microcomputed tomography and conventional histomorphometry. Calcif Tissue Int 1997;61:493-8.
34. Ibrahim N, Parsa A, Hassan B, et al. Diagnostic imaging of trabecular bone microstructure for oral implants: a literature review. Dentomaxillofac Radiol 2013;42:20120075.
35. Scarfe WC, Farman AG. What is cone-beam CT and how does it work? Dent Clin North Am 2008;52:707-30, v.
36. Scarfe WC, Farman AG, Sukovic P. Clinical applications of cone-beam computed tomography in dental practice. J Can Dent Assoc 2006;72:75-80.
37. Molteni R. Prospects and challenges of rendering tissue density in Hounsfield units for cone beam computed tomography. Oral Surg Oral Med Oral Pathol Oral Radiol 2013;116:105-19.
38. Katsumata A, Hirukawa A, Okumura S, et al. Relationship between density variability and imaging volume size in cone-beam computerized tomographic scanning of the maxillofacial region: an in vitro study. Oral Surg Oral Med Oral Pathol Oral Radiol Endod 2009;107:420-5.
39. Schulze R, Heil U, Gross D, et al. Artefacts in CBCT: a review. Dentomaxillofac Radiol 2011;40:265-73.
40. Mozzo P, Procacci C, Tacconi A, et al. A new volumetric CT machine for dental imaging based on the cone-beam technique: preliminary results. Eur Radiol 1998;8:1558-64.
41. Ludlow JB, Davies-Ludlow LE, Brooks SL, et al. Dosimetry of 3 CBCT devices for oral and maxillofacial radiology: CB Mercuray, NewTom 3G and i-CAT. Dentomaxillofac Radiol 2006;35:219-26.
42. Ketcham RA, Carlson WD. Acquisition, optimization and interpretation of X-ray computed tomographic imagery: applications to the geosciences. Comput Geosci 2001;27:381-400.
43. Barrett JF, Keat N. Artifacts in CT: recognition and avoidance. Radiographics 2004;24:1679-91.
44. Feldkamp LA, Davis LC, Kress JW. Practical cone-beam algorithm. J Opt Soc Am A 1984;1:612-9.
45. Siltanen S, Kolehmainen V, Järvenpää S, et al. Statistical inversion for medical x-ray tomography with few radiographs: I. General theory. Phys Med Biol 2003;48:1437-63.
46. Bryant JA, Drage NA, Richmond S. Study of the scan uniformity from an i-CAT cone beam computed tomography dental imaging system. Dentomaxillofac Radiol 2008;37:365-74.
47. Mah P, Reeves TE, McDavid WD. Deriving Hounsfield units using grey levels in cone beam computed tomography. Dentomaxillofac Radiol 2010;39:323-35.
48. Reeves TE, Mah P, McDavid WD. Deriving Hounsfield units using grey levels in cone beam CT: a clinical application. Dentomaxillofac Radiol 2012;41:500-8.
49. Rührnschopf EP, Klingenbeck K. A general framework and review of scatter correction methods in x-ray cone-beam computerized tomography. Part 1: Scatter compensation approaches. Med Phys 2011;38:4296-311.
50. Dong X, Petrongolo M, Niu T, et al. Low-dose and scatter-free cone-beam CT imaging using a stationary beam blocker in a single scan: phantom studies. Comput Math Methods Med 2013;2013:637614.
51. Li J, Yao W, Xiao Y, et al. Feasibility of improving cone-beam CT number consistency using a scatter correction algorithm. J Appl Clin Med Phys 2013;14:4346.
52. Staub D, Murphy MJ. A digitally reconstructed radiograph algorithm calculated from first principles. Med Phys 2013;40:011902.
53. Hunter AK, McDavid WD. Characterization and correction of cupping effect artefacts in cone beam CT. Dentomaxillofac Radiol 2012;41:217-23.
54. Nomura Y, Watanabe H, Honda E, et al. Reliability of voxel values from cone-beam computed tomography for dental use in evaluating bone mineral density. Clin Oral Implants Res 2010;21:558-62.
55. Naitoh M, Hirukawa A, Katsumata A, et al. Evaluation of voxel values in mandibular cancellous bone: relationship between cone-beam computed tomography and multislice helical computed tomography. Clin Oral Implants Res 2009;20:503-6.
56. Parsa A, Ibrahim N, Hassan B, et al. Reliability of voxel gray values in cone beam computed tomography for preoperative implant planning assessment. Int J Oral Maxillofac Implants 2012;27:1438-42.
57. Parsa A, Ibrahim N, Hassan B, et al. Bone quality evaluation at dental implant site using multislice CT, micro-CT, and cone beam CT. Clin Oral Implants Res 2013.
58. Pittman JW, Navalgund A, Byun SH, et al. Primary migration of a mini-implant under a functional orthodontic loading. Clin Oral Investig 2014;18:721-8.
59. Cha JY, Kil JK, Yoon TM, et al. Miniscrew stability evaluated with computerized tomography scanning. Am J Orthod Dentofacial Orthop 2010;137:73-9.
60. Huang H, Richards M, Bedair T, et al. Effects of orthodontic

treatment on human alveolar bone density distribution. Clin Oral Investig 2013;17:2033-40.
61. Taylor TT, Gans SI, Jones EM, et al. Comparison of micro-CT and cone beam CT-based assessments for relative difference of grey level distribution in a human mandible. Dentomaxillofac Radiol 2013;42:25117764.
62. Agbaje JO, Jacobs R, Maes F, et al. Volumetric analysis of extraction sockets using cone beam computed tomography: a pilot study on ex vivo jaw bone. J Clin Periodontol 2007;34:985-90.
63. Huja SS, Beck FM. Bone remodeling in maxilla, mandible, and femur of young dogs. Anat Rec (Hoboken) 2008;291:1-5.
64. Kennedy KS, Jones EM, Kim DG, et al. A prospective clinical study to evaluate early success of short implants. Int J Oral Maxillofac Implants 2013;28:170-7.
65. Leblebicioglu B, Salas M, Ort Y, et al. Determinants of alveolar ridge preservation differ by anatomic location. J Clin Periodontol 2013;40:387-95.
66. Benavides E, Rios HF, Ganz SD, et al. Use of cone beam computed tomography in implant dentistry: the International Congress of Oral Implantologists consensus report. Implant Dent 2012;21:78-86.
67. Santiago RC, de Paula FO, Fraga MR, et al. Correlation between miniscrew stability and bone mineral density in orthodontic patients. Am J Orthod Dentofacial Orthop 2009;136:243-50.
68. Song YD, Jun SH, Kwon JJ. Correlation between bone quality evaluated by cone-beam computerized tomography and implant primary stability. Int J Oral Maxillofac Implants 2009;24:59-64.
69. Aranyarachkul P, Caruso J, Gantes B, et al. Bone density assessments of dental implant sites: 2. Quantitative cone-beam computerized tomography. Int J Oral Maxillofac Implants 2005;20:416-24.
70. Guerrero ME, Jacobs R, Loubele M, et al. State-of-the-art on cone beam CT imaging for preoperative planning of implant placement. Clin Oral Investig 2006;10:1-7.
71. Hsu JT, Chen YJ, Tsai MT, et al. Predicting cortical bone strength from DXA and dental cone-beam CT. PLoS One 2012;7:e50008.
72. Hsu JT, Chang HW, Huang HL, et al. Bone density changes around teeth during orthodontic treatment. Clin Oral Investig 2011;15:511-9.
73. dos Anjos Pontual ML, Freire JS, Barbosa JM, et al. Evaluation of bone changes in the temporomandibular joint using cone beam CT. Dentomaxillofac Radiol 2012;41:24-9.
74. Hohlweg-Majert B, Metzger MC, Kummer T, et al. Morphometric analysis - Cone beam computed tomography to predict bone quality and quantity. J Craniomaxillofac Surg 2011;39:330-4.
75. Loubele M, Maes F, Schutyser F, et al. Assessment of bone segmentation quality of cone-beam CT versus multislice spiral CT: a pilot study. Oral Surg Oral Med Oral Pathol Oral Radiol Endod 2006;102:225-34.
76. Nackaerts O, Depypere M, Zhang G, et al. Segmentation of Trabecular Jaw Bone on Cone Beam CT Datasets. Clin Implant Dent Relat Res 2014.
77. Hangartner TN. Thresholding technique for accurate analysis of density and geometry in QCT, pQCT and microCT images. J Musculoskelet Neuronal Interact 2007;7:9-16.
78. Klintstrom E, Smedby O, Moreno R, et al. Trabecular bone structure parameters from 3D image processing of clinical multi-slice and cone-beam computed tomography data. Skeletal Radiol 2014;43:197-204.
79. Wang L, Chen KC, Gao Y, et al. Automated bone segmentation from dental CBCT images using patch-based sparse representation and convex optimization. Med Phys 2014;41:043503.
80. Burghardt AJ, Link TM, Majumdar S. High-resolution computed tomography for clinical imaging of bone microarchitecture. Clin Orthop Relat Res 2011;469:2179-93.
81. Loubele M, Jacobs R, Maes F, et al. Image quality vs radiation dose of four cone beam computed tomography scanners. Dentomaxillofac Radiol 2008;37:309-18.
82. Link TM. Osteoporosis imaging: state of the art and advanced imaging. Radiology 2012;263:3-17.

http://dx.doi.org/10.11005/jbm.2014.21.2.117